JOURNAL OF MATERIALS SCIENCE **34** (1999) 5879–5884

Densification model for powder compacts

DAVID C. C. LAM
Dept. of Mechanical Engineering, Hong Kong University of Science and Technology, Clear Water Bay, Kowloon, Hong Kong
E-mail: medcclam@ust.hk

The driving force of densification has traditionally been modeled on the basis of local curvature changes between powder particle pairs. Extension of particle pair analysis to powder compacts involving billions of particles has not been successful because of the geometric difference between the two cases. In this paper, a densification stress model for grain boundary and lattice diffusion controlled densification is developed on the basis of a powder compact's thermodynamics and the internal surface area evolution. For compacts with a constant grain size, the model predicts that the densification stress increases as a function of relative density, which is in agreement with experimental trends. With grain growth, the densification stress becomes relatively constant throughout the intermediate stage of densification, in agreement with experimental data in the literature. Comparison of densification rate data with densification rate model employing the developed densification stress relation also gives good functional agreement. These agreements indicate that modelling densification stress and densification rate on the basis of internal surface area captures the essential physics of powder compact densification. © *1999 Kluwer Academic Publishers*

1. Introduction

Powder based parts are typically sintered at high temperature to eliminate voids and to strengthen the parts. The sintering process is driven by a decrease in the overall potential energy via reduction of the solid-vapor interfacial energy in balance with the growth of solid-solid interfaces within the part (Fig. 1). The sintering process can be loosely divided into three stages: the initial stage covers the growth of necks between touching particles, the second or intermediate stage is characterized by a continuous interconnected network of both pore and solid phases, and the final stage commences when the pores are no longer continuous, but are broken into isolated pores.

In the initial and intermediate stage, necks are formed between touching particles owing to potential gradients between the particle surfaces and the contact points. For a pair of identically sized single crystalline spheres, the neck between the two particles will grow until an energy balance between the decreasing solid-vapor surface energy and increasing solid-solid grain boundary energy is established. The growth of the neck during this period can occur via surface, grain boundary and volume diffusion or vapor transport via evaporation and condensation (Fig. 2). In the initial stage at low temperature, surface diffusion does not contribute to densification (no movement between particle mass centers) but will contribute strongly to neck formation because of its low activation energy. At higher temperature, grain boundary and volume diffusion will be activated to eliminate void space between particles. Based on these diffusion mechanisms, a number of sintering models describing

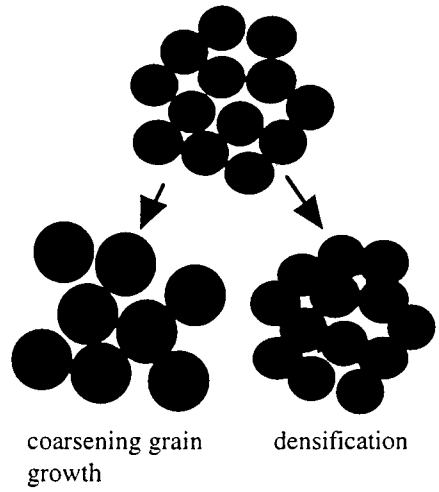

Figure 1 Schematic of the decrease in the overall potential energy via reduction of the solid-vapor interfacial area (densification) or via reduction of particle/grain area via grain growth and coarsening.

the evolution of neck geometry between two particles or an array of particles have been developed [1–4]. The sintering driving force is principally modeled on the basis of the local particle and neck curvature. Sintering laws describing the evolution of neck geometry developed on this basis compare well with neck growth experiments. However, extension of the pair model to the densification of a powder compact has met with less success [5]. The divergence between model and experiments can be attributed to previously unaccounted geometric changes in a compact. For example, local particle rearrangements [6], new contact formation and

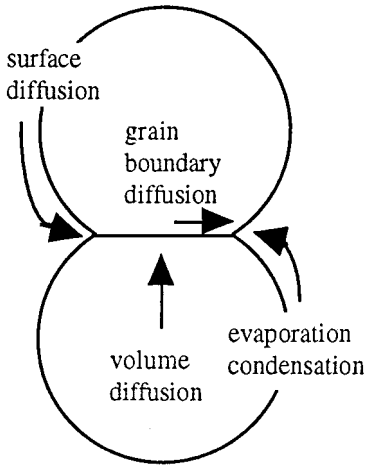

Figure 2 Schematic of densification mechanisms (after Helle [12]).

differential sintering owing to local density variations [7] have been found to affect the development of sintering bodies.

In the intermediate stage, the microstructure resembles a partially compacted assembly of copper spheres. The deformed particles form an interconnected network penetrated by an interconnected network of pores. By modeling the intermediate stage microstructure as an interconnected network of polyhedra and cylindrical pores, Coble [8] has been able to model the sintering driving force and develop densification rate equations for lattice diffusion and grain boundary diffusion. However, the equations are applicable to a small density range in which the grain size and pore geometry remain relatively constant. Chu *et al.* [9] modeled the densification behavior of a cubic array of spheres for a wide density range while using a constant densification stress.

Recently, progress in hot isostatic pressing (HIPing) of powder compacts has added a new prespective onto pressureless sintering. In HIPing, the external pressure is isostatically applied to the entire compact causing the compact to densify via high temperature creep. The behavior of the compact has been modeled based on diffusion mechanisms [10, 11]. HIPing maps were generated and reasonable agreements were found between the models and HIPing experiments [12].

Pressureless sintering can also be viewed as creep, but with the compressive pressure provided by the compact's tendency to reduce total compact surface energies. Constitutive laws for sintering have been developed on the basis of the creep behavior of porous compacts while still employing the driving force relation developed for the initial stage sintering of an array of spheres and final stage sintering of a microstructure containing isolated pores [13]. The intermediate stage of sintering, where more than 50% of the densification shrinkage occurs, is largely ignored. In the following section, a sintering driving force relation formulated on the basis of energy changes associated with surface area fraction is developed. Then, the relation is incorporated into diffusion equations to give a fully microstructural based densification relation for powder compacts for comparisons with experimental densification stress and densification rate data in the literature.

2. Densification stress model

Sintering is driven by the tendency of the compact to reduce the solid-vapor surface and grain boundary area. Representing the solid-vapor surface energy per unit area and the grain boundary energy per unit area as γ_s and γ_{gb}, the potential energy of a unit single crystalline particle in a powder compact is given as

$$E = \gamma_s A_s + \frac{\gamma_{gb}}{2} A_{gb} \tag{1}$$

where A_s and A_{gb} are respectively the surface-vapor surface area and grain boundary area of the particle, and the factor of two is introduced because grain boundary area is shared by two particles. Defining A as the solid-vapor surface area fraction per unit particle

$$A = \frac{A_s}{A_s + A_{gb}}, \tag{2}$$

and V_m as the mass volume, the particle surface area-volume relation can be written as

$$\frac{A_s + A_{gb}}{V_m} = \frac{\alpha}{G} \tag{3}$$

where α is the shape factor for the particle (6 for spheres) and G is the characteristic particle size. Combining the three equations gives

$$E = \left[\gamma_s A + \frac{\gamma_{gb}}{2}(1 - A)\right]\frac{\alpha}{G} V_m. \tag{4}$$

γ_s and γ_{gb} are related to the equilibrium dihedral angle Φ_e through

$$\frac{\gamma_{gb}}{\gamma_s} = 2\cos\left(\frac{\Phi_e}{2}\right). \tag{5}$$

Defining k as the cosine and substituting into Equation 4 gives

$$E = [k + A(1 - k)]\frac{\alpha}{G}\gamma_s \rho V_b \tag{6}$$

after rearrangement. For equiaxed particles, shape factor α can be assumed to remain constant throughout sintering. With k and γ_s defined as material constants, the differential change in potential energy as a function of microstructural changes is simply

$$\frac{dE}{dV_b} = \frac{\partial E}{\partial G}\frac{\partial G}{\partial V_b} + \frac{\partial E}{\partial A}\frac{\partial A}{\partial V_b} + \frac{\partial E}{\partial \rho}\frac{\partial \rho}{\partial V_b} + \frac{\partial E}{\partial V_b}. \tag{7}$$

But since

$$V_b = \frac{V_m}{\rho}. \tag{8}$$

and V_m is constant for a compact, Equation 7 reduces to

$$\frac{dE}{dV_b} = \frac{\partial E}{\partial G}\frac{\partial G}{\partial V_b} + \frac{\partial E}{\partial A}\frac{\partial A}{\partial V_b} \tag{9}$$

The term on the left hand side is the overall driving pressure for microstructural change during sintering while the first term on the right hand side is the driving stress for grain growth and the second term on the right hand side is the driving stress for change in surface area fraction. Defining P_d as the densification stress

$$P_d = \frac{\partial E}{\partial A}\frac{\partial A}{\partial V_b} \tag{10}$$

and substituting Equation 6 for A gives

$$P_d = -\frac{\alpha\gamma_s\rho^2(1-k)}{G}\frac{\partial A}{\partial \rho}, \tag{11}$$

after simplification. G and A are functions of the microstructure, separately accounting for grain growth and coarsening, and the effect of surface area changes without grain growth on P_d, respectively.

The evolution of surface area A_s in sintered metal powder has been studied by Rhines *et al.* [14]. They concluded that the surface area A_s for a compact in the intermediate stage of sintering should be a linear function of relative density. Artz [15] studied the evolution of A_{gb} analytically and measured the grain boundary area of powder compacts isostatically compacted to different densities. Both their data and analysis revealed that grain boundary area varies linearly as a function of relative density from the initial as-packed state to the fully compacted state. Shaw and Brook [16] measured the evolution of surface area and grain boundary area during sintering for pure alumina compacts and alumina compacts with MgO additive to control alumina's grain growth. Transforming their data into area fraction A using Equation 2 reveals that surface area fraction is a linear function of relative density (Fig. 3). The data for alumina with and without MgO are collinear despite their different grain growth behavior. Clearly, A and G are separable functions and surface area fraction A can be modeled as a function of relative density

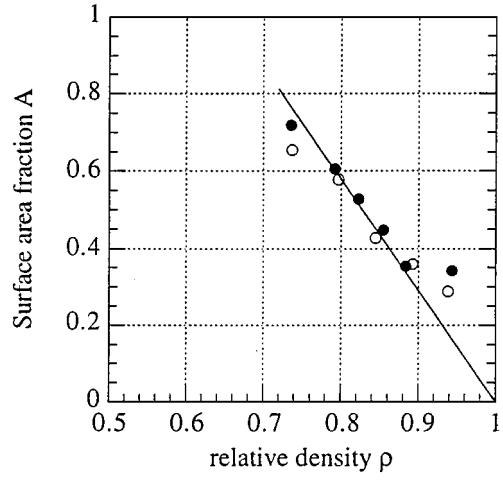

Figure 3 Plot of surface area fraction for Al_2O_3 (○) and Al_2O_3 doped with grain growth controlling MgO (●). The plotted points are calculated from surface area measurements from Shaw and Brook [16]. The surface area fraction is collinear in spite of the different grain growth behavior.

independent of grain size with the equation

$$A = \xi\frac{1-\rho}{1-\rho_o}. \tag{12}$$

At $\rho = 1$, the sintered body is fully dense and the surface area fraction must be zero. When the body is in the initial state with $\rho = \rho_o$, A is equal to ξ. If there is no appreciable surface diffusion to the neck before densification commences, the compact can be assumed to have no appreciable neck area and ξ is equal to one. For typical powder compacts, ξ can be approximately taken as 0.9 ± 0.1, to account for particle neck thickening owing to surface diffusion or evaporation-condensation. Substituting Equation 12 into 11 and simplifying gives

$$P_d = \alpha\gamma_s(1-k)\frac{A\rho^2}{G(1-\rho)} \tag{13}$$

where the P_d is a function of material constants and evolving microstructural parameters.

3. Densification rate

Under densification stress, mass is removed from grain boundary regions to the pore surfaces, resulting in densification. Powder compact densification rate under a given densification stress has been developed by Wilkinson [17], Artz [18] and Chu *et al.* [9]. Chu *et al.* derived a pressureless densification rate relation for cubically packed array of spheres while Arzt, building on Wilkinson's work developed a densification relation from detailed consideration of the evolving particle geometries in a random dense packed compact under isostatic pressure (HIPing). Following Wilkinson and Artz for a randomly packed compact, the rate of solid volume removal from the boundary (neck) region per unit particle under a given densification is

$$\frac{dV_{m,gb}}{dt} = \frac{4\pi D\Omega Z P_{eff}}{k_B T} \tag{14}$$

where D is the sum of the lattice diffusion coefficient and the product of grain boundary diffusion coefficient times grain boundary thickness, Ω is the atomic volume, Z is the average particle coordination number and k_B is the Boltzman's constant. The effective stress acting at the grain boundary P_{eff} is related to the densification stress P_d [19] through

$$P_{eff} = \frac{P_d}{\rho(1-A)} \tag{15}$$

where $(1-A)$ is the grain boundary area fraction. The displacement rate per sintered contact is simply the removal rate (Equation 15) divided by the grain boundary area. Normalizing displacement rate by the mean particle radius ($G/2$) gives

$$\dot{\varepsilon} = \frac{d\varepsilon}{dt} = \frac{2}{G}\frac{dV_{m,gb}}{A_{gb}\,dt} \tag{16}$$

where $\dot{\varepsilon}$ is the average true strain rate of the compact. Since

$$\dot{\rho} = 3\rho\dot{\varepsilon}, \tag{17}$$

the densification rate is simply

$$\dot{\rho} = \frac{24\rho D\Omega Z P_{\text{eff}}}{G^3 k_{\text{B}} T(1-A)} \tag{18}$$

after substitution. Taking $Z = 12\rho$ from Helle *et al.* [12] and combining Equations 15 into 18 gives

$$\dot{\rho} = \frac{288\rho D\Omega P_{\text{d}}}{G^3 k_{\text{B}} T(1-A)^2} \tag{19}$$

Typically, P_{d} is an empirical constant in the range of 1–10 MPa. With the new model for densification stress, a new rate law can be written. Substituting for P_{d} using Equation 13 gives the new fully microstructural based densification rate law as

$$\dot{\rho} = \Pi \frac{\rho^3 A}{G^4(1-\rho)(1-A)^2} \tag{20a}$$

with

$$\Pi = \frac{288 D\Omega\alpha\gamma_{\text{s}}(1-k)}{k_{\text{B}} T}, \tag{20b}$$

where Π is the aggregate temperature dependent material constant.

4. Comparisons and discussion

The functional dependence of the densification stress on the microstructure is embodied in the material constant Π, surface area fraction A, relative density ρ, and grain size G in the current model. Direct experimental data on densification stress as a function of the evolving microstructure in terms of G, ρ and A are sparse. Rhines *et al.* [14] experimentally measured the uniaxial densification of a copper powder compact during the initial stage of sintering where grain size remained constant. The measured stress was found to increase as a function of relative density. For densification with no grain growth, the theoretical densification stress P_{d} (Equation 13) is a monotonically increasing function of relative density (Fig. 4). Thus, the densification model is in qualitative agreement with stress measurements on the initial stage sintering of copper powders with constant grain size. The increase is a natural consequence of the increase in energy density as the body densifies (ρ^2 term in Equation 11). While P_{d} is dependent on surface area fraction, but it does not contribute to the increase in the densification since the rate of change of A with respect to ρ (Equation 11) is constant. In real compacts with growing grains, the rise in densification stress is counter-balanced by the inverse dependence on G.

The functional dependence of densification stress on grain growth is not directly available, but can be obtained indirectly from densification rate and creep rate

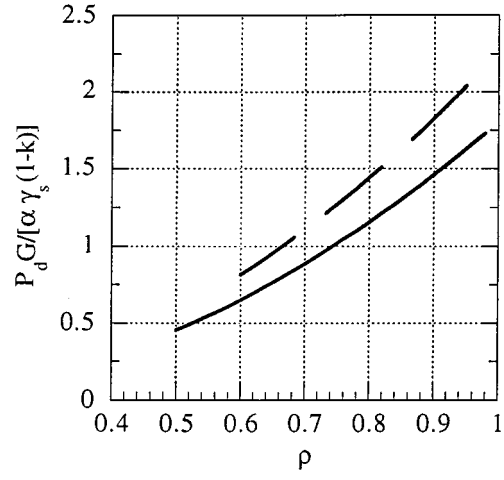

Figure 4 Normalized densification stress curves for compacts with initial relative densities of 0.5 (solid curve) and 0.6 (dashed curve), assuming constant grain size.

data. Chu *et al.* [9] reported densification rate and constant load creep rate during the intermediate stage of sintering for CdO, ZnO, MgO, MgO with Bi_2O_3 and $YBa_2Cu_3O_2$ powder compacts for varying conditions of temperature and initial and sintered densities. They found that the ratio densification rate/creep rate generally exhibited a slight decrease when plotted as a function of relative density with the exception of MgO with Bi_2O_3, which exhibited a small rise. Creep rate is dependent on the applied creep load and creep viscosity of the compact, while the densification rate is dependent on the densification stress and densification viscosity. Theoretical analysis of the ratio of creep viscosity to densification viscosity suggested that the ratio is nearly constant independent of sintered density [20]. On this basis, Chu *et al.* [9] concluded from their densification/creep rate data that the densification stress is also relatively constant for a wide range of relative densities and temperatures.

In the current model, a constant densification stress would result if G, the grain growth term counterbalances the rise due to the ρ^2 term. Consider CdO compacts in which grain size [21] varies according to the empirically fitted equation (Fig. 5a)

$$G = 15.68 - 44.1\rho + 34.9\rho^2 \quad (0.7 \leq \rho \leq 0.9) \tag{22}$$

for CdO compacts with initial relative density $\rho_{\text{o}} = 0.58$ (Fig. 5a). The predicted densification stress P_{d} with grain growth is plotted along with experimentally measured densification stress for CdO compacts (Fig. 5b). Good functional agreement is obtained between the data and the theoretical relation (Equation 11). The densification stress without grain growth (G fixed at 1.84 μm: extrapolated grain size at $\rho_{\text{o}} = 0.58$ using Equation 22) is plotted for comparison (Fig. 5c). Without grain growth, the stress is predicted to increase from ~2 MPa to ~3 MPa. With grains growing from 2 μm to ~4 μm (Fig. 5a), the densification stress decreased from ~2 MPa to ~1.5 MPa. As was observed by Chu *et al.* [9] for a wide variety of material systems, the increase in grain size counter-balanced the

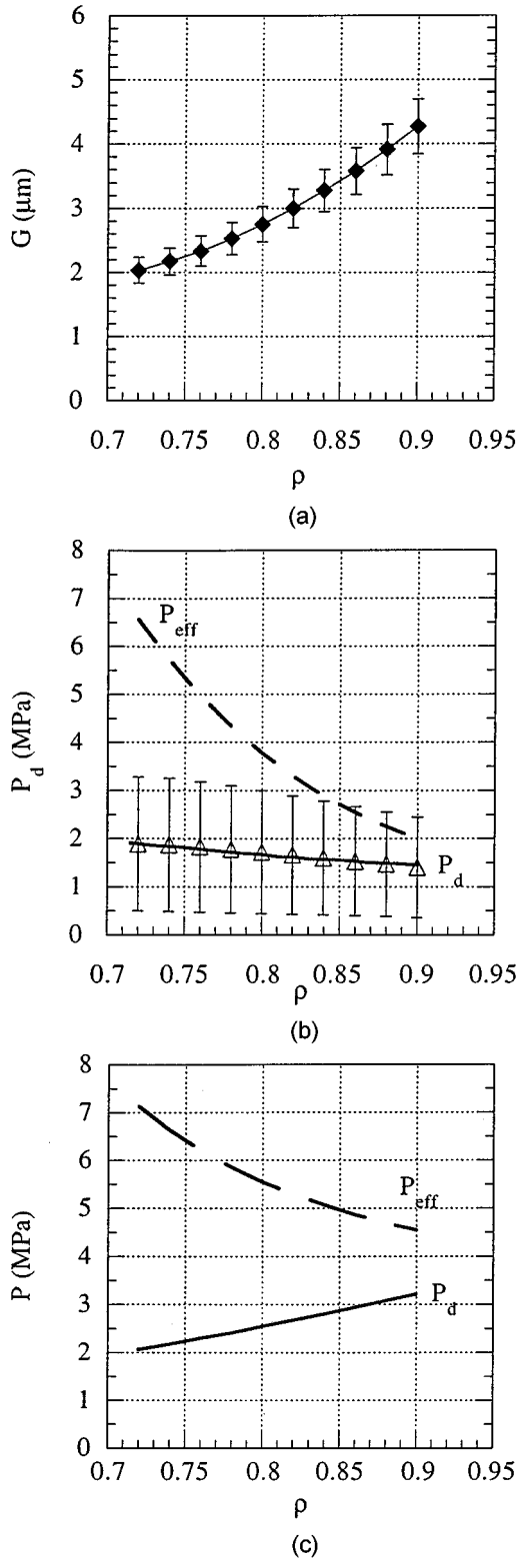

Figure 5 (a) CdO grain size data plotted with 20% error and curve fit. (b) Comparison of densification stress as predicted by the model (P_d, bold solid curve) with CdO experimental data (△) derived from creep strain and densification rate [21]. Error in P_d was estimated from CdO grain size measurement error which is reported to be 20% (G curve). The effective stress at grain junction is also plotted for comparison (P_{eff}). $\rho_o = 0.58$; $\Phi = 130^\circ$, and $\gamma_s = 1$ J/m^2 are use for material constants. (c) Theoretical prediction of densification stress (P_d) and effective densification stress (P_{eff}) for CdO with grain size held at $G = 1.84\,\mu$m, $\rho_o = 0.58$; $\Phi = 130^\circ$, and $\gamma_s = 1$ J/m^2.

ρ^2 term, resulting in approximately constant densification stress for CdO powder compacts. Clearly, if grain growth is inhibited by additives, as in the case for MgO doped with Bi_2O_3, an increasing densification stress as

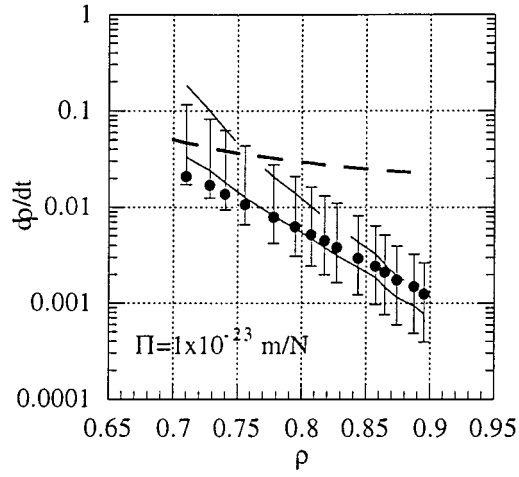

Figure 6 Direct comparison of densification rate (solid curve) predicted by model with densification rate data (●) for CdO compacts [21] with $\rho_o = 0.58$, $\Phi = 130^\circ$, $\gamma_s = 1$ J/m^2, and $\Pi = 1 \times 10^{-23}$ m/N. Error bars for the data were calculated on the basis of the reported 20% error in grain size measurement. The long dashed curve represents the model's prediction when ρ_o is increased to 0.68. The short dashed curve represents the model's prediction when the grain size G is fixed and held at 1.84 μm with $\rho_o = 0.58$.

a function of relative density, as reported by Chu *et al*. [9] is not unexpected.

The new densification rate relation (Equation 20a) incorporating the new densification stress model can be directly compared with CdO powder compact densification rate data [21]. The predicted densification rate along with the rate data is plotted in Fig. 6. The model systematically overestimated the data at low density and underestimated the densification rate at high density. The systematic error may have originated from modeling errors in surface area fraction A, densification stress formulation and experimental error. Since densification stress has compared well with data, the stress formulation and surface area fraction model A are unlikely error sources. Systematic experimental error in grain size measurement is the likely source as the densification rate is strongly dependent on it via a 4th power dependence. Small measurement error in G will not affect densification stress, but will dramatically affect densification rate. Thus with a reported 20% error in grain size measurement (plotted error bars), the agreement between the model and data is acceptable within given error.

5. Microstructural dependence

The effect of microstructural parameters on the densification rate are varied and explored in this section. Densification rate is dependent on the material constants, grain size and surface area fraction. Both grain size and surface area fraction is in turn dependent on the sintered relative density ρ and initial compact density ρ_o. The effect of initial density on densification rate is shown in Fig. 6. Increasing the initial compact relative density ρ_o from 0.58 to 0.68 increases the densification rate by 500% at $\rho = 0.7$ (long dashed curve in Fig. 6). At $\rho = 0.9$, the densification rate for $\rho_o = 0.68$

case decreased to approximately 150% of the rate for $\rho_o = 0.58$ case. Hence increasing initial density generally enhances densification rate, but the enhancement diminishes with progressive densification.

The theoretical densification rate with no grain growth ($G = 1.84\ \mu$m) is plotted as a short dashed curve (Fig. 6). Without grain growth, the densification rate is relatively constant with densification rate at $\rho = 0.9$ diminish by only 50% relative to the densification rate at $\rho = 0.7$ (short dashed curve). With grain growth, the densification rate at $\rho = 0.90$ is less than 10% of the rate at $\rho = 0.7$ (solid curve). Clearly, increasing initial relative density can boost densification rate, perhaps in the first half of densification, while grain growth control can elevate the densification rate throughout densification.

6. Conclusion

A new densification stress model has been developed in place of traditional pairwise models. Observed experimental trends were explained by the new model and comparison with experimentally measured densification stress in the literature gave good agreement. Densification rate relation developed on the same basis gave reasonable functional agreement between experimental data and model. Agreements in both densification stress and densification rate models suggest that for a given material, the densification process is strongly affected by initial relative density mainly in the first half of densification while grain growth affects the densification throughout.

References

1. G. C. KUCZYNSKI, *Met. Trans. AIME*. **185** (1949) 169.
2. W. D. KINGERY and M. BERG, *J. Appl. Phys*. **26** (1955) 1205.
3. R. L. COBLE, *J. Amer. Ceram. Soc*. **41** (1958) 55.
4. R. M. GERMAN and Z. A. MUNIR, "Sintering and Catalysis, Mat. Sci. Res." Vol. 10 edited by G. C. Kucyznski, (Plenum Press, New York, 1975) p. 249.
5. D. L. JOHNSON and I. B. CULTER, *J. Amer. Ceram. Soc*. **46** (1963) 542.
6. H. E. EXNER, *Rev. Powd. Met. Phys. Ceram*. **1** (1979) 1.
7. R. K. BORDIA and G. W. SCHERER, *Acta Metall*. **36** (1988) 2393.
8. R. L. COBLE, *J. Appl. Phys*. **36** (1965) 2327.
9. M.-Y. CHU, L. C. DEJONGHE and M. N. RAHAMAN, *Acta Metall*. **37** (1989) 1415.
10. C. H. HSEUH, A. G. EVANS, R. M. CANON and R. J. BROOK, *Acta Metall*. **34** (1986) 927.
11. R. M. MCMEEKING and L. T. KUHN, *Acta Metall. Mater*. **40** (1992) 961.
12. A. S. HELLE, K. E. ESTERLING and M. F. A, *ibid*. **26** (1985) 2163.
13. Z. Z. DU and A. C. F. COCKS, *ibid*. **40** (1992) 1969.
14. F. N. RHINES, R. T. DEHOFF and R. A. RUMMEL, "Agglomeration," edited by W. A. Knepper (Interscience, London, 1962) 391.
15. E. ARTZ, *Acta Metall*. **30** (1982) 1883.
16. N. J. SHAW and R. J. BROOK, *J. Amer. Ceram. Soc*. **69** (1986) 107.
17. D. S. WILKINSON, PhD thesis, University of Cambridge 1977.
18. E. ARZT, M. F. ASHBY and K. E. EASTERLING, *Metall. Trans. A* **14A** (1983) 211.
19. A. S. HELLE, K. E. EASTERLING and M. F. ASHBY, *Acta Metall*. **33** (1985) 2163.
20. G. W. SCHERER, *J. Amer. Ceram. Soc*. **70** (1987) 719.
21. M. N. RAHAMAN, L. C. DEJONGHE and R. J. BROOK, *ibid*. **69** (1986) 53.

Received 10 March 1997
and accepted 18 June 1999